AD

TECHNICAL REPORT ARCCB-TR-96027

INTERNAL STRESSES, TEXTURE, AND ANISOTROPY IN HIGH-CONTRACTION ELECTROPLATED CHROMIUM COATINGS

S. L. LEE
G. P. CAPSIMALIS

SEPTEMBER 1996

US ARMY ARMAMENT RESEARCH,
DEVELOPMENT AND ENGINEERING CENTER
CLOSE COMBAT ARMAMENTS CENTER
BENÉT LABORATORIES
WATERVLIET, N.Y. 12189-4050

DISCLAIMER

The findings in this report are not to be construed as an official Department of the Army position unless so designated by other authorized documents.

The use of trade name(s) and/or manufacturer(s) does not constitute an official indorsement or approval.

DESTRUCTION NOTICE

For classified documents, follow the procedures in DoD 5200.22-M, Industrial Security Manual, Section II-19 or DoD 5200.1-R, Information Security Program Regulation, Chapter IX.

For unclassified, limited documents, destroy by any method that will prevent disclosure of contents or reconstruction of the document.

For unclassified, unlimited documents, destroy when the report is no longer needed. Do not return it to the originator.

REPORT DOCUMENTATION PAGE

Form Approved
OMB No. 0704-0188

1. AGENCY USE ONLY (Leave blank)	2. REPORT DATE	3. REPORT TYPE AND DATES COVERED
	September 1996	Final

4. TITLE AND SUBTITLE
INTERNAL STRESSES, TEXTURE, AND ANISOTROPY IN HIGH-CONTRACTION ELECTROPLATED CHROMIUM COATINGS

5. FUNDING NUMBERS
AMCMS No. 6226.24.H180.0
PRON No. TU5A5F361AFP

6. AUTHOR(S)
S.L. Lee and G.P. Capsimalis

7. PERFORMING ORGANIZATION NAME(S) AND ADDRESS(ES)
U.S. Army ARDEC
Benet Laboratories, AMSTA-AR-CCB-O
Watervliet, NY 12189-4050

8. PERFORMING ORGANIZATION REPORT NUMBER
ARCCB-TR-96027

9. SPONSORING/MONITORING AGENCY NAME(S) AND ADDRESS(ES)
U.S. Army ARDEC
Close Combat Armaments Center
Picatinny Arsenal, NJ 07806-5000

10. SPONSORING/MONITORING AGENCY REPORT NUMBER

11. SUPPLEMENTARY NOTES
Presented at the 44th Annual Denver X-Ray Conference, Colorado Springs, CO, 31 July - 4 August 1995.
Published in *Advances in X-Ray Analysis*, Volume 39, 1996.

12a. DISTRIBUTION/AVAILABILITY STATEMENT
Approved for public release; distribution unlimited.

12b. DISTRIBUTION CODE

13. ABSTRACT (Maximum 200 words)

Internal residual stresses in refractory coatings of the bore cause cracking, flaking, peeling, and failure of the coatings and substrate. Strong <111> fiber texture, perfect in-plane azimuthal symmetry, low single-crystal anisotropy, and high-surface tensile residual stresses were observed in high-contraction chromium on steel. The conventional d-sin$^2\Psi$ method fails in the evaluation of residual stress if the existence of texture is not taken into account. Elastic moduli were evaluated from single-crystal elastic constants. Two methods were developed to extract residual stresses in textured chromium coatings:

- A new matlab matrix inversion method using a single family of reflections. The method allows calculation of residual stress and unstrained lattice parameter in textured cubic materials.
- A Hill-Neerfeld model assuming elastic isotropy. This is a d-sin$^2\Psi$ method adapted to multiple families of reflections.

14. SUBJECT TERMS
Electrolytic Chromium Deposition, Refractory Coatings, Chromium Elastic Moduli, Residual Stress

15. NUMBER OF PAGES
20

16. PRICE CODE

17. SECURITY CLASSIFICATION OF REPORT	18. SECURITY CLASSIFICATION OF THIS PAGE	19. SECURITY CLASSIFICATION OF ABSTRACT	20. LIMITATION OF ABSTRACT
UNCLASSIFIED	UNCLASSIFIED	UNCLASSIFIED	UL

TABLE OF CONTENTS

TABLE OF CONTENTS
(Continued)

FIGURES

Acknowledgements

The author appreciates the efforts of J. Cox, M. Miller, S. Langston, and F. Yee in preparing the laboratory chromium specimens; A. Kapusta for electron microscopy work; and Dr. A. Winholtz and Dr. A. Christensen for their technical advice.

INTRODUCTION

High-contraction chromium is plated on A723 steel bore by an aqueous electrolytic process to extend the wear and erosion life of the gun tube. Chromium has been extensively used in industry to reduce galling, friction, wear, and erosion. It has a high melting point, high hardness, low coefficient of friction, and is chemically inert to hot propellant gases. However, production electrolytic chromium coatings suffer from extensive cracks, which result from high internal stresses generated during the electrolytic deposition process. During operation, the cracks grow due to the high thermal and tensile stress cycling condition and the aggressive chemical environment of the bore. The cracks allow hot propellant gases, such as CO, CO_2, H_2, N_2, and H_2O, to penetrate the deposition and interact with the substrate, causing failure of the coatings and substrate. Analysis of quantitative texture and residual stress is critical in the study of crack formation and coating quality.

Benet Laboratories' research in the electrolytic chromium plating process is summarized in several reports and references.[1-4] Recent investigators showed high surface-tensile residual stresses in chromium electroplating.[5-9] In this work, strong <111> fiber texture with almost perfect in-plane azimuthal symmetry and high tensile residual stresses were observed in production electrolytic chromium coatings. Anisotropy factor and the aggregate elastic moduli were calculated from single-crystal elastic constants. Two methods were used to determine residual stress in textured chromium coatings:

- A new Matlab matrix inversion method based on the Reuss uniform stress model was developed to determine residual stress and unstrained lattice parameter.

- A Hill-Neerfeld isotropic elastic model using the d-$\sin^2\Psi$ method adapted to multiple families of reflections. The d-$\sin^2\Psi$ method for residual stress analysis normally fails in textured material. However, in high-contraction chromium coatings, deviation from linearity was not severe.

HIGH-CONTRACTION CHROMIUM DEPOSITION PROCESS

High-contraction chromium bore plating used an immersion electrolytic plating technique. The plating solution was made of 256 gm/liter CrO_3, 2.56 gm/liter H_2SO_4, plus distilled water. Plating temperature was 55°C, and current density was 30 amp/dm^2. Cathode current efficiency was approximately 11%. The substrate material was A723 steel. The current immersion chromium plating technique and the improved flow-through chromium vessel plating technique are described in a previous technical report.[10]

EXPERIMENTAL PROCEDURE

Two laboratory chromium specimens, lab-hc-a2 and lab-hc-fy, were plated on 10 x 50 x 1 mm A723 steel coupons, using the same immersion solution, current density, and temperature as in the production chromium plating process. The production chromium specimen S213 was obtained by chromium plating a 120-mm 1-inch thick ring of A723 steel in the production immersion tank. It was then subjected to post-plating heat treatment at 425°C for four hours for hydrogen relief. A 1-in^2 specimen was cut from the ring to facilitate X-ray evaluation. Knoop hardness measurements of high-contraction chromium specimens gave approximately 1,000 ±55. A Leitz metallography microscope measured the coating thicknesses of the specimens.

Texture and residual stress analyses were performed using a four-axis Scintag diffractometer with a χ-tilt goniometer, where the tilts are around an axis parallel to the diffractometer plane. Reflected X-rays were observed using a Kevex-Peltier-cooled solid-state detector. Pole figures were obtained using χ range of 0° to 80° at 5° steps, and ϕ range of 0° to 360° at 5° steps. For precision diffraction peak location determination, the diffraction peaks were fitted to Pearson VII peak profile.

FIBER TEXTURE IN PRODUCTION CHROMIUM COATINGS

In Figure 1, a 2θ scan for production chromium specimen S213 is compared with a scan for 140 mesh stress-free chromium powder using copper radiation. These scans show predominately preferred [111] orientations in the chromium coatings on steel. Also shown in Figure 1 is the 2θ scan of the Fe substrate of S213 compared with 400 mesh stress-free iron powder. These scans show that the A723 steel substrate has near random crystalline orientation.

In Figure 2, Cr(110), Cr(200), and Cr(211) pole figures are shown. These pole figures were obtained for production specimen S213 using chromium radiation. These pole figures demonstrate predominately <111> fiber texture with random in-plane orientation in production chromium on steel. Interplane angles are (111)/(110) = 35° and (111)/(200) = 55°, producing the rings observed. Two rings were observed in the (211) pole figure due to the interplane angles (111)/(211) = 20° and (111)/(2,1,-1) = 62°.

In Figure 3, the angular relations between the planes are further illustrated by 2θ scans using chromium radiation. A surface scan of production specimen S213 shows no diffraction peaks. Tilting the specimen to χ = 19.5° brought up the (211) reflection. Tilting the specimen to χ = 35.3° brought up the (110) reflection. Tilting the specimen to χ = 54.7° brought up the (200) reflection.

REFLECTIONS USED IN RESIDUAL STRESS ANALYSIS

The differential form of Bragg's law is plotted in Figure 4, giving the locations for Cr<211>, Cr<200>, Cr<110>, Cu<222>, Cu<310>, Cu<220>, Cu<211>, Cu<200>, and Cu<110> peaks. The curve shows that percentage errors become very large for small 2θ angles.

Because of the strong preferred orientation, few reflections in the back reflection region have strong intensities for residual stress analysis. Table 1 gives the radiations and reflections used in the residual stress analysis of fiber-textured chromium coatings. Residual stress analysis used reflections from multiple families of crystallographic planes and radiations from both Cr and Cu tubes.

PROBLEMS OF STRESS DETERMINATION IN TEXTURED CHROMIUM

Many scientists have studied residual stress analysis in textured materials. Noyan and Cohen,[11] Van Houtte and De Buyser[12] and References 3-15 quoted within summarize these efforts. However, there are problems in determining residual stress in textured materials using the conventional $\sin^2\Psi$ method because:

- Texture reduces intensity at certain Ψ- angles (χ - angle used in this work). Because of the preferred orientation, many reflections are not available for residual stress analysis.
- Nonlinearity in the d-$\sin^2\Psi$ plot due to elastic anisotropy.
- Lateral and depth gradients in stress and texture.
- Inhomogeneous distribution of elastic residual strains.

Figure 5 shows this study's attempt to determine residual stress in high-contraction chromium using conventional $\sin^2\Psi$ techniques. Scans of 2θ are obtained for the <222> peak at 135.4° using Cu radiation for Ψ = -45° to 45° at 7 steps. The method obviously fails because the only diffraction peak that appears is for Ψ = 0°. The pole figures show that because of the high degree of texture, diffraction peaks appear only at specific tilt angles.

In the following sections, two methods for residual stress analysis in textured chromium are described:

- A Matlab matrix inversion method based on the Reuss uniform stress model.
- A Hill-Neerfeld isotropic model, which is used to calculate the X-ray elastic constants for the $\sin^2\Psi$ evaluation of residual stress.

MATLAB MATRIX INVERSION METHOD

Residual stress analysis in textured cubic crystals is simplified considerably when the specimen normal is a specific crystallographic direction.[13-15] Clemens and Bain[13] assumed a Reuss average and derived equations to extract residual stress and unstrained lattice parameter from measured strains. The technique is applicable to fiber-textured or epitaxial thin films with cubic structure, when the crystallographic texture is such that the specimen normal is in the [111], [110], or [001] direction. Using their equation for the case of <111> fiber texture and equal biaxial stress where $\sigma = \sigma_{11} = \sigma_{22}$, a 2 x 2 matrix is set up to solve for the unknowns σ and d_o. In the nonequal biaxial case, a similar method can be used to solve for σ_{11}, σ_{22}, and d_o by setting up a 3 x 3 matrix. Assuming an equal biaxial stress state, the relation between residual stress, unstrained lattice parameter, and measured residual strain is reduced to the following equation. Other researchers have used a similar equation to analyze biaxial residual stress in <111> fiber textured coatings.[8,9,16,17]

$$(d_\Psi - d_o)/d_o = \sigma[(2s_{11} + 4s_{12} - s_{44})/3 + (s_{44} \sin^2 \Psi/2)] \quad (1)$$

where d_Ψ is the d-spacing measured at tilt Ψ, d_o is the unstrained lattice parameter, σ is biaxial stress, and the s_{ij} terms are the compliance tensor components. In this work, a matrix inversion method is developed to calculate residual stress and unstrained lattice parameter from Equation (1). Consider two d-spacing measurements $d_{\Psi 1}$ and $d_{\Psi 2}$ made at two Ψ values Ψ_1 and Ψ_2, where

$$k_1 = (2s_{11} + 4s_{12} - s_{44})/3, \; k_{21} = s_{44} \sin^2 \Psi_1/2, \text{ and } k_{22} = s_{44} \sin^2 \Psi_2/2$$

Equation (1) can be rewritten in two equations:

$$d_{\Psi 1} = \sigma d_o [\, k_1 + k_{21} \,] + d_o \quad (2)$$

$$d_{\Psi 2} = \sigma d_o [\, k_1 + k_{22} \,] + d_o \quad (3)$$

Thus, in the biaxial case, a 2 x 2 matrix is sufficient to solve for the unknowns σ and d_o:

$$\begin{matrix} \sigma d_o \\ d_o \end{matrix} = \begin{matrix} k_1 + k_{21} & 1 \\ k_1 + k_{22} & 1 \end{matrix}^{-1} \begin{matrix} d_{\Psi 1} \\ d_{\Psi 2} \end{matrix} \quad (4)$$

In practice, two measurements were made on the specimen surface, one longitudinal and one transverse, with an arbitrary choice of orientation. Table 2 gives the results of the analysis using Cr radiation. This method of residual stress analysis uses a single family of reflections. It

minimizes diffractometer alignment error and systematic error associated with 2θ measurements. Anticipated errors are expected to be less than ±10 Ksi. The same technique can be used to obtain residual stress using other reflections listed in Table 1.

SINGLE-CRYSTAL ANISOTROPY

Maximum and minimum elastic moduli in single crystals can be found in the referenced literature. For example, elastic modulus for copper in the [111] direction is 2.85 times that in the [100] direction; in silver and gold, the ratio is 2.66, and in alpha-iron, 2.15. According to Noyan and Cohen,[11] Young's modulus for hkl planes in cubic crystals is given by:

$$1/E_{hkl} = S_{11} - 2[(S_{11} - S_{12}) - S_{44}/2](a_{11}^2 a_{12}^2 + a_{12}^2 a_{13}^2 + a_{11}^2 a_{13}^2)$$

where a_{ij} are direction cosines between the crystal axes and the direction [hkl]. Table 3 gives the compliance coefficients for chromium at room temperature along with our calculated Young's modulus and elastic anisotropy factor $A = 2*(S_{11} - S_{12})/S_{44}$. Young's modulus exhibits a maximum along the [100] direction and a minimum along the [111] direction in bcc chromium.

AGGREGATE ELASTIC CONSTANTS

In a macroscopically isotropic or weak textured aggregate polycrystalline material, Young's modulus and Poisson's ratio can be calculated from single-crystal elastic constants assuming linear elastic models. Existing elastic models include Voigt,[18] Reuss,[19] Hill,[20] Neerfeld,[21] Hashin,[22] and Shtrikman,[23] and Kröner's self-consistent model.[24] Hill-Neerfeld showed that Voigt's uniform strain model and Reuss's uniform stress model are the least upper bound and greatest lower bound of the elastic constants, and suggested using their mean. Hashin and Shtrikman's calculations gave closer upper and lower bounds between Voigt's and Reuss's models. Kröner's model led to an intermediate solution between the models of Reuss and Voigt. Table 4 provides this study's calculation of elastic moduli. Since the Hill-Neerfeld model is easy to perform and has sufficient accuracy, it is used in the residual stress evaluation.

HILL-NEERFELD ISOTROPIC MODEL

Assuming an isotropic crystalline distribution, the Hill-Neerfeld model was used to calculate elastic constants for $\sin^2\psi$ evaluation of residual stress using multiple planes of reflections. Figure 6 shows the results of residual stress analysis using both chromium and copper radiations. The X-ray elastic constant $S_2 = \nu/E$ was calculated for each reflection using spreadsheet software. Residual stress measurement using copper tube alone is 94 Ksi and 88 Ksi using combined copper and chromium tubes. Goodness of fit gave an error estimate of approximately ±15 Ksi. Mass absorption coefficient in chromium for Cu Kα is three times that for Cr Kα. However, depth of penetration did not significantly affect the residual stress levels.

Recent studies by Pina et al. and Cassagne using Cu and Fe radiations give comparable high surface tensile residual stresses in chromium.[8,9]

TOPOGRAPHY AND MICROSTRUCTURE IN PRODUCTION CHROMIUM

Figure 7 shows scanning electron microscope surface topography and microstructure analysis of high-contraction chromium. The left two images are from microstructural analysis showing extensive cracks due to high internal stresses. In general, chromium cracks vary in size and are up to 1 micron wide, and 5-10 microns long. Surface topography in the right two images shows fibrous columnar grains.

CONCLUSIONS

As a result of this study, we may draw the following conclusions:

- Production high-contraction chromium coatings exhibit strong <111> fiber-texture and random in-plane crystallite orientation.
- Matlab matrix inversion evaluation of biaxial residual stresses in two laboratory specimens lab-hc-a2 and lab-hc-fy gave 80 Ksi, 86 Ksi, production specimen S213, which when heat-treated gave 41 Ksi. The errors are estimated at ±10 Ksi.
- Hill-Neerfeld $\sin^2\Psi$ stress evaluation of the laboratory specimen lab-hc-a2 using calculated elastic X-ray constants adapted to multiple families of reflections gave 88 Ksi. Estimated errors are ±15 Ksi.
- Texture influences residual stress in that only reflections at specific Ψ's are observed and available for residual stress analysis. Chromium is highly textured and $\sin^2\Psi$ should not be used. However, results show no significant deviation from linearity in the $\sin^2\Psi$ plot.
- The high-tensile stresses measured in the coating surfaces correlate well with the extensive cracks observed in production high-contraction chromium on steel.

REFERENCES

1. Chen, E. S., Capsimalis, G. P., and Weigle, G. R., U.S. Army ARDEC Technical Report ARCCB-TR-85002, Benet Laboratories, Watervliet, NY, January 1985.

2. Todaro, M. E., Capsimalis, G. P., and Chen, E. S., U.S. Army ARDEC Technical Report ARCCB-TR-87007, Benet Laboratories, Watervliet, NY, March 1987.

3. Pan, S. K., Miller, M. D., and Nelson, F. J., U.S. Army ARDEC Technical Report ARCCB-TR-89024, Benet Laboratories, Watervliet, NY, October 1989.

4. Miller, M. D. and Pan, S. K., U.S. Army ARDEC Technical Report ARCCB-TR-90014, Benet Laboratories, Watervliet, NY, April 1990.

5. Baron, H. U. and Hauk, V., *Z. Metallk*, Volume 79, No. 2, 1988, pp. 127-131.

6. Lee, S. L., presented at Gordon Research Conference on NDE, Henniker, NH, 29 June-3 July 1994.

7. Lee, S. L., Christensen, A., and Robie, S., Scintag Application Notes 940403, Scintag Inc., Sunnyvale, CA, 1994.

8. Pina, J., Dias, A., Francois, M., and Lebrun, J. L., *Proceedings of SEM Fourth International Conference on Residual Stresses*, 1994, pp. 742-751.

9. Cassagne, V., Lebrun, J. L., and Le Cornec, A., *Proceedings of SEM Fourth International Conference on Residual Stresses*, 1994, pp. 752-757.

10. Collins, L., U.S. Army ARDEC Technical Report ARCCB-TR-93014, Benet Laboratories, Watervliet, NY, 1993.

11. Noyan, I. C. and Cohen, J. B., Residual Stress: Measurement by Diffraction and Interpretation, Springer-Verlag, NY, 1987.

12. Van Houtte, P. and De Buyser, L., *Acta Met. Mat.*, Vol. 41, No. 2, 1993, pp. 323-336.

13. Clemens, B. M. and Bain, J. A., *MRS Bulletin*, July 1992, pp. 46-51.

14. Hauk, V. and Vaessen, G., *Z. Metallk*, Vol. 71, 1985, p. 102.

15. Tanaka, K., Ishihara, K., and Akiniwa, Y., presented at Denver X-Ray Conference, Denver, CO, 1995.

16. Korhonen, M. A. and Paszkiet, C. A., *Scripta Met.*, Vol. 23, 1989, pp. 1449-1454.

17. Zaouali, M., Lebrun, J. L., and Gergaud, P., *Sur. Coat. Technology*, Vol. 50, 1991, pp. 5-10.

18. Voigt, W., Lehrbuch der Kristallphysik, Teubner, Leipzig/Berlin, 1928.

19. Reuss, A., *Z. Angew. Math. Mech.*, Vol. 9, 1929, pp. 49-58.

20. Hill, R., *Proc. Phy. Soc.*, Vol. A65, 1952, pp. 349-354.

21. Neerfeld, H., *Mitt. KWI Eisenforsch*, Vol. 24, 1942, p. 61.

22. Hashin, Z., *J. Mech. Phys. Solids*, Vol. 10, 1962, p. 343.

23. Shtrikman, S., *J. Mech. Phys. Solids,* Vol. 11, 1963, p. 127.

24. Kröner, E., *J. Mech. Phys. Solids,* Vol. 15, 1967, pp. 319-329.

Table 1. Radiations and reflections used in fiber-textured chromium residual stress analysis

X-ray	hkl planes	2θ	χ - tilt
CR	211	153°	+/- 19.5°
CR	211	153°	+/- 61.9°
CU	222	135°	0°
CU	222	135°	+/- 70.5°
CU	310	115°	+/- 43.1°
CU	310	115°	+/- 68.6°

Table 2. Matlab residual stress analysis in textured coatings

Sample	Thickness	X-ray	Stress (Ksi)	d_o (Å)
lab-hc-a2	2.5 mil	Cr	80	1.17779
lab-hc-fy	1.8 mil	Cr	86	1.17786
S213	4.8 mil	Cr	41	1.17784

Table 3. Single-crystal elastic constants S_{ij} ($x10^{10}$ pascal^{-1}) and calculation of Young's modulus E_{hkl} (GPa) and anisotropy factor in chromium at room temperature

S_{11}	S_{12}	S_{44}	E_{100}	E_{111}	E_{110}	A
0.03004	-0.00487	0.09774	332.903	254.239	270.150	0.714

Table 4. Calculation of Young's modulus (GPa) and Poisson's ratio in chromium crystalline aggregates

Elastic Constants	Voigt	Reuss	Hill-Neerfeld	Shtrikman bound	Hashin bound
Young's modulus	286.93	280.73	283.83	283.57	283.98
Poisson's ratio	0.2089	0.2153	0.2121	0.2123	0.2119

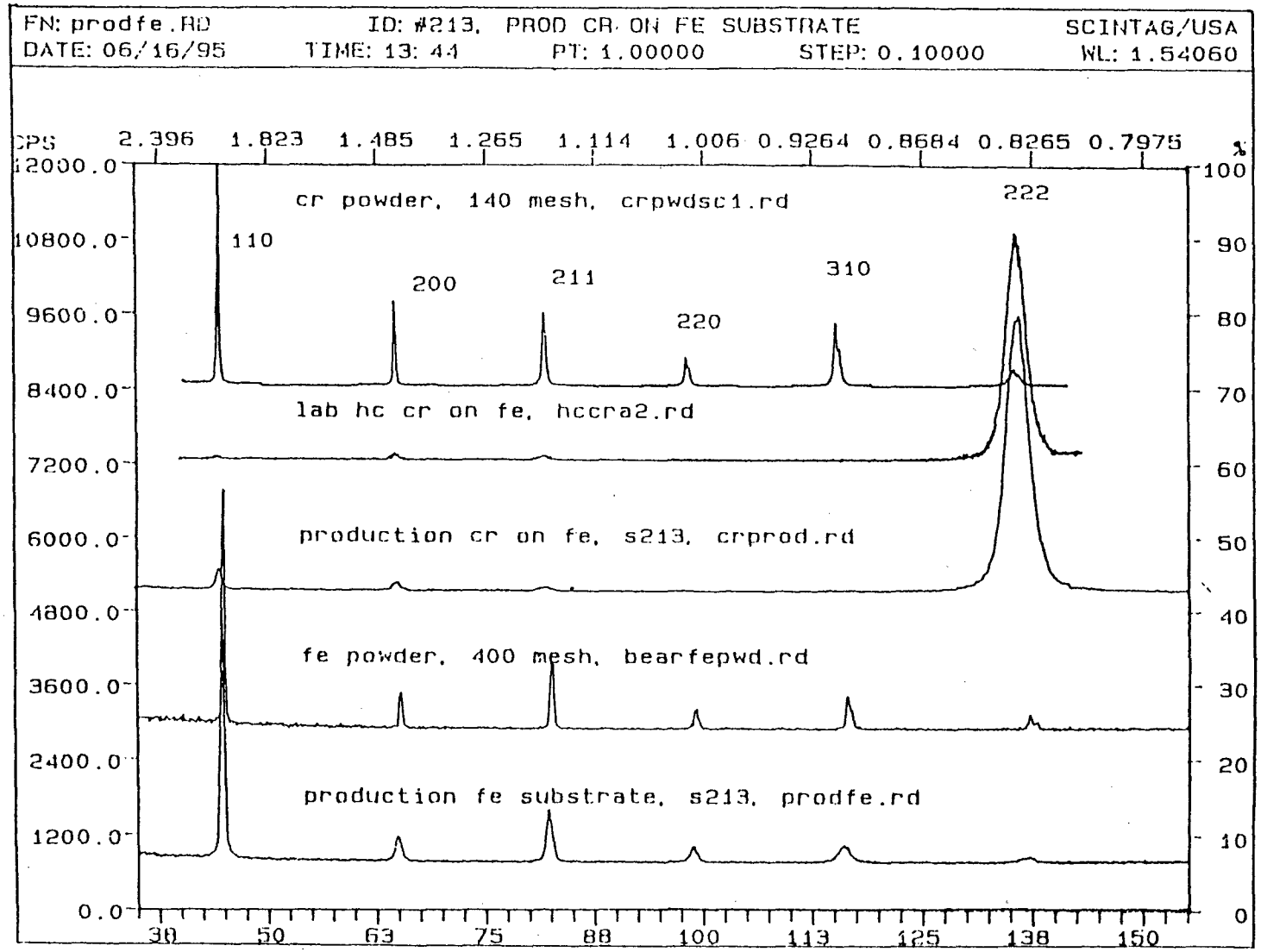

Figure 1. 2θ scans of production Cr coatings on steel compared with Cr powder and steel substrate bore compared with Fe powder

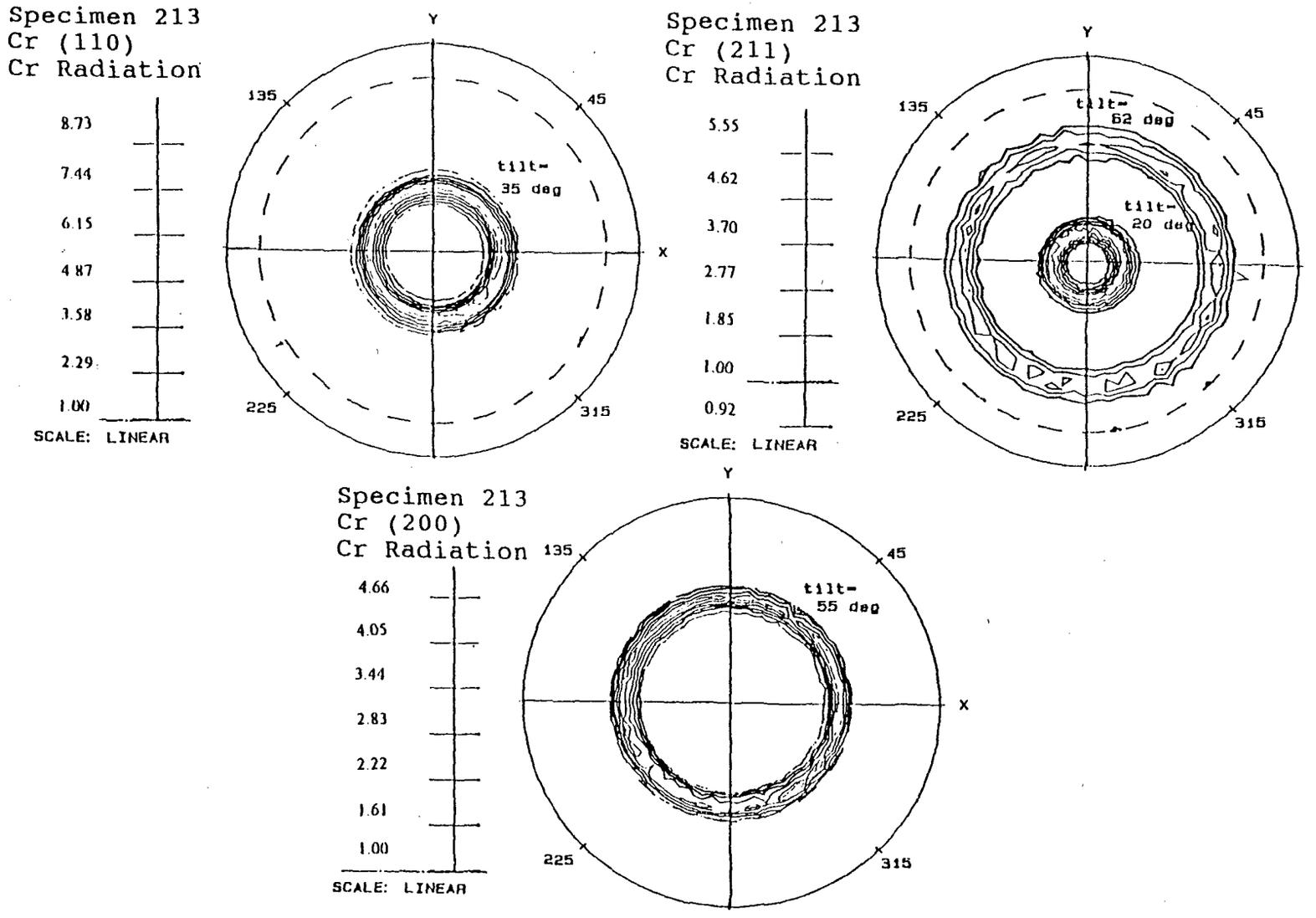

Figure 2. Cr(110), Cr(211), and Cr(200) pole figures using Cr K_α radiation, showing strong fiber texture in production chromium coatings on A723 steel substrate

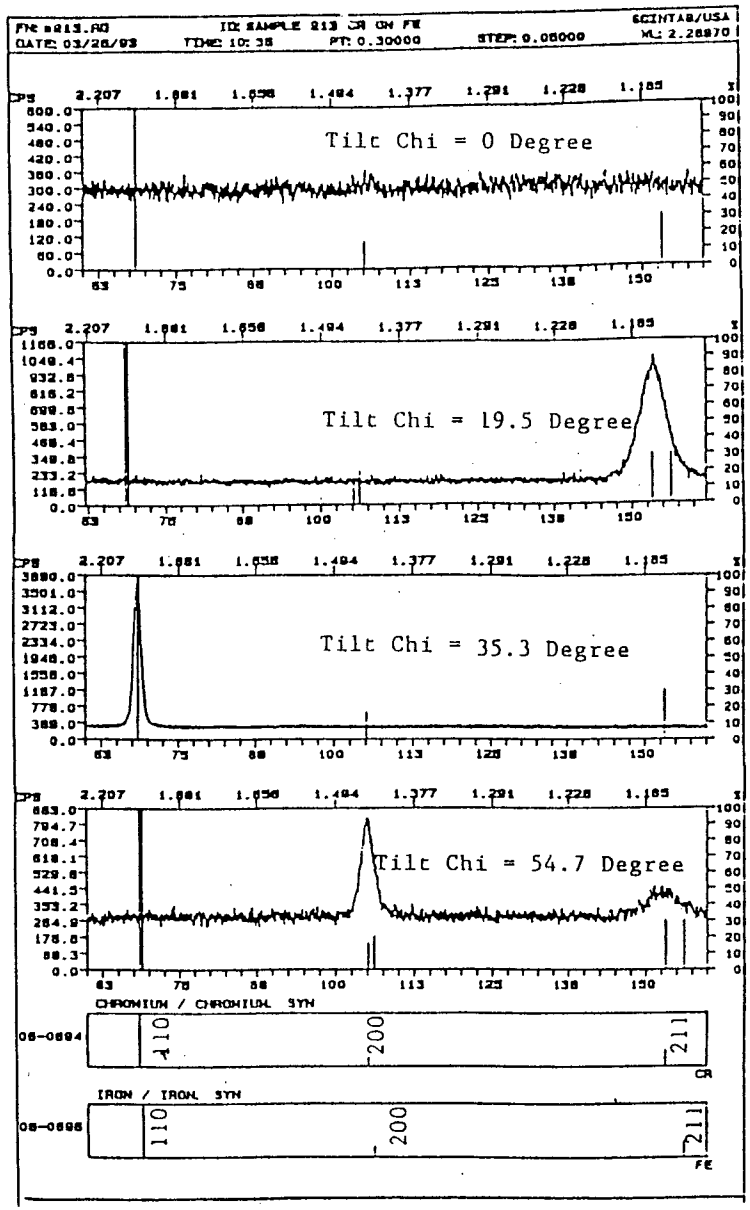

Figure 3. 2θ scans of production Cr specimen on steel at specific χ- tilts, showing the appearance of the (211), (110), and (200) reflections. ICDD database is shown on the bottom. Cr K_α radiation was used.

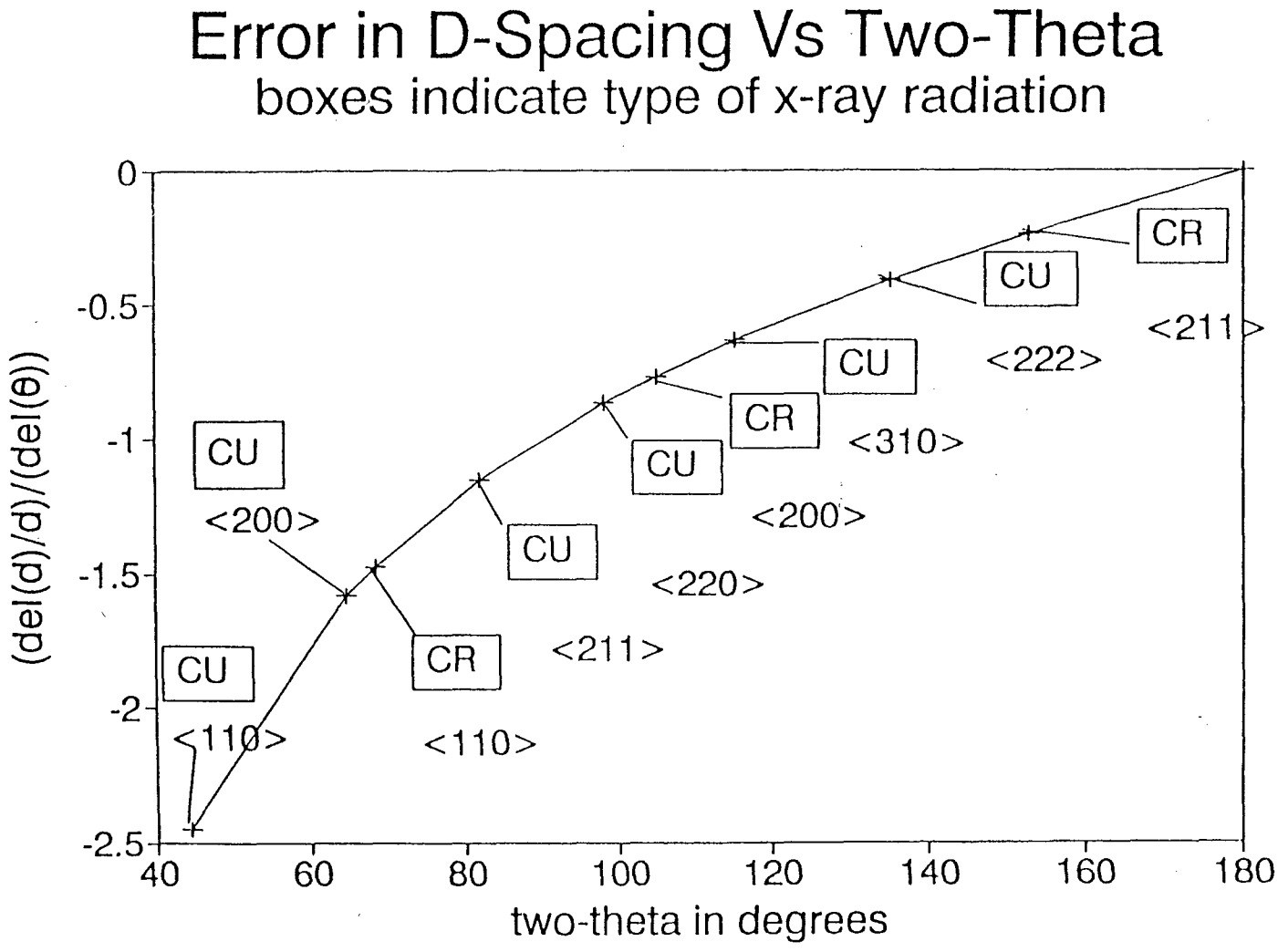

Figure 4. Differential form of Bragg's law showing relative error versus 2θ for residual stress analysis

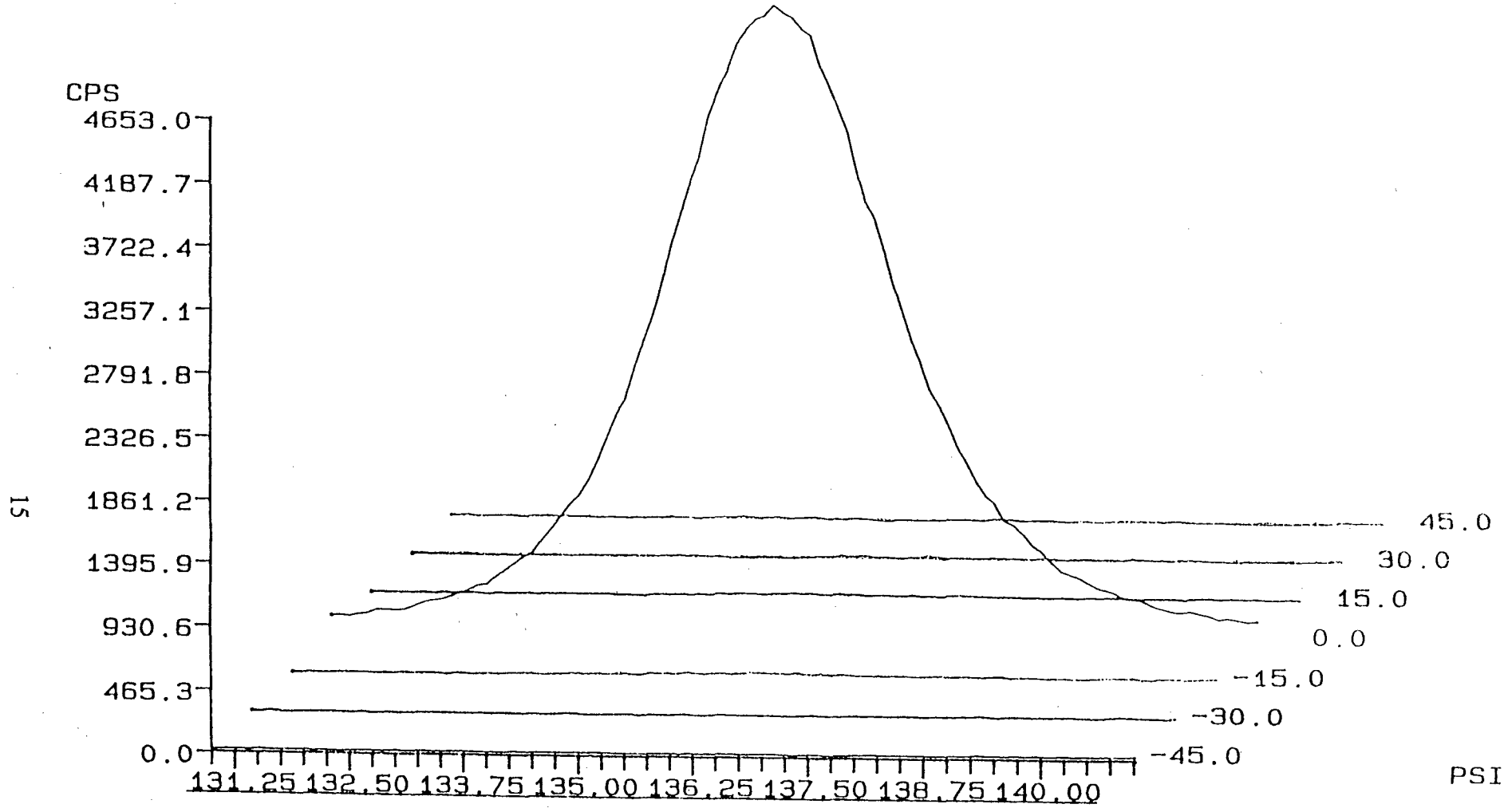

Figure 5. Three-dimensional plot of conventional d-sin$^2\Psi$ biaxial residual stress determination using Cr<222> peak at 2θ = 135.42°, χ = -45° to 45° using Cu radiation-failed because diffraction peak appeared only at χ = 0°

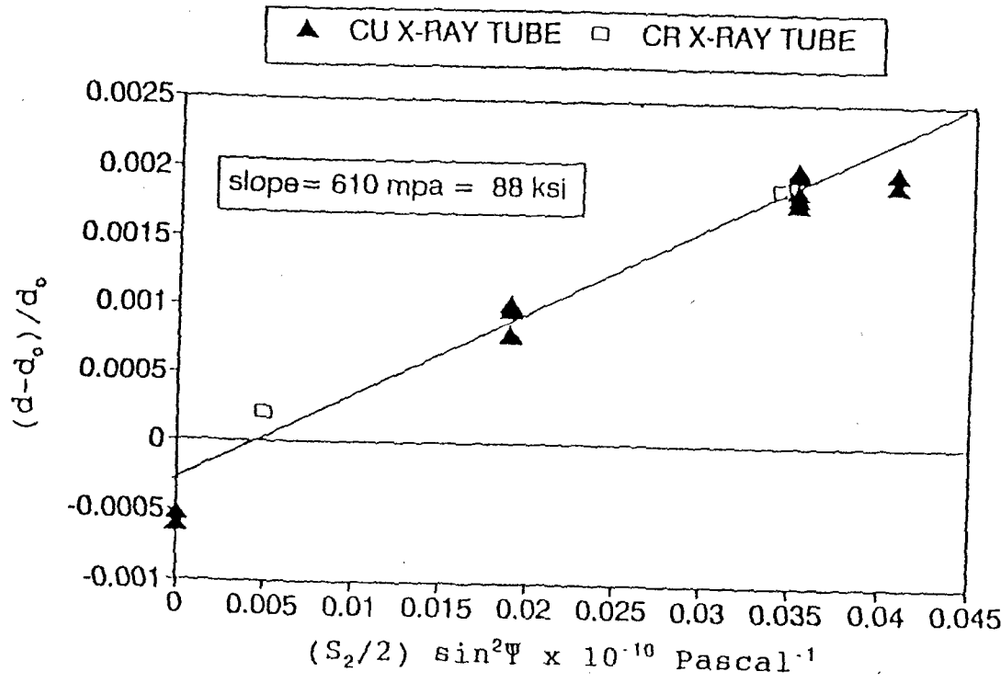

Figure 6. Residual stress analysis in textured chromium using Cr and Cu radiations

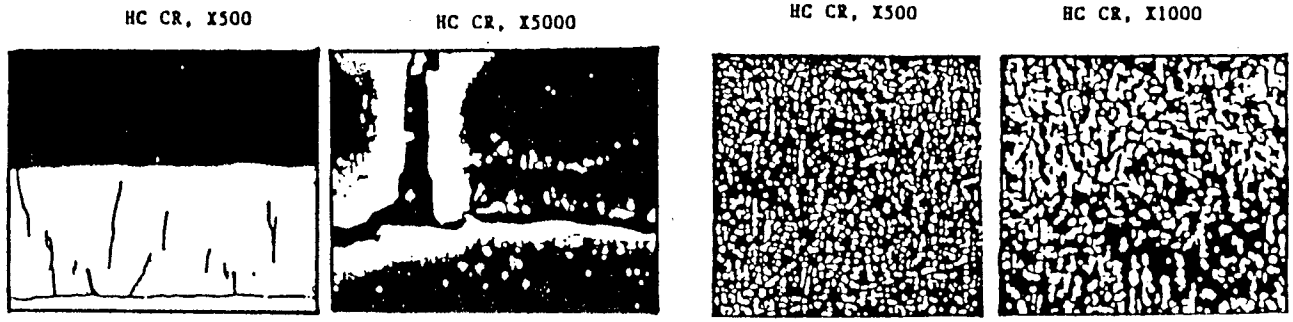

Figure 7. Surface topology and microstructure in high-contraction chromium electrolytic deposition

TECHNICAL REPORT INTERNAL DISTRIBUTION LIST

	NO. OF COPIES
CHIEF, DEVELOPMENT ENGINEERING DIVISION	
ATTN: AMSTA-AR-CCB-DA	1
-DB	1
-DC	1
-DD	1
-DE	1
CHIEF, ENGINEERING DIVISION	
ATTN: AMSTA-AR-CCB-E	1
-EA	1
-EB	1
-EC	1
CHIEF, TECHNOLOGY DIVISION	
ATTN: AMSTA-AR-CCB-T	2
-TA	1
-TB	1
-TC	1
TECHNICAL LIBRARY	
ATTN: AMSTA-AR-CCB-O	5
TECHNICAL PUBLICATIONS & EDITING SECTION	
ATTN: AMSTA-AR-CCB-O	3
OPERATIONS DIRECTORATE	
ATTN: SIOWV-ODP-P	1
DIRECTOR, PROCUREMENT & CONTRACTING DIRECTORATE	
ATTN: SIOWV-PP	1
DIRECTOR, PRODUCT ASSURANCE & TEST DIRECTORATE	
ATTN: SIOWV-QA	1

NOTE: PLEASE NOTIFY DIRECTOR, BENÉT LABORATORIES, ATTN: AMSTA-AR-CCB-O OF ADDRESS CHANGES.

TECHNICAL REPORT EXTERNAL DISTRIBUTION LIST

	NO. OF COPIES
ASST SEC OF THE ARMY RESEARCH AND DEVELOPMENT ATTN: DEPT FOR SCI AND TECH THE PENTAGON WASHINGTON, D.C. 20310-0103	1
DEFENSE TECHNICAL INFO CENTER ATTN: DTIC-OCP (ACQUISITIONS) 8725 JOHN J. KINGMAN ROAD STE 0944 FT. BELVOIR, VA 22060-6218	2
COMMANDER U.S. ARMY ARDEC ATTN: AMSTA-AR-AEE, BLDG. 3022	1
AMSTA-AR-AES, BLDG. 321	1
AMSTA-AR-AET-O, BLDG. 183	1
AMSTA-AR-FSA, BLDG. 354	1
AMSTA-AR-FSM-E	1
AMSTA-AR-FSS-D, BLDG. 94	1
AMSTA-AR-IMC, BLDG. 59 PICATINNY ARSENAL, NJ 07806-5000	2
DIRECTOR U.S. ARMY RESEARCH LABORATORY ATTN: AMSRL-DD-T, BLDG. 305 ABERDEEN PROVING GROUND, MD 21005-5066	1
DIRECTOR U.S. ARMY RESEARCH LABORATORY ATTN: AMSRL-WT-PD (DR. B. BURNS) ABERDEEN PROVING GROUND, MD 21005-5066	1
DIRECTOR U.S. MATERIEL SYSTEMS ANALYSIS ACTV ATTN: AMXSY-MP ABERDEEN PROVING GROUND, MD 21005-5071	1
COMMANDER ROCK ISLAND ARSENAL ATTN: SMCRI-SEM ROCK ISLAND, IL 61299-5001	1
MIAC/CINDAS PURDUE UNIVERSITY 2595 YEAGER ROAD WEST LAFAYETTE, IN 47906-1398	1
COMMANDER U.S. ARMY TANK-AUTMV R&D COMMAND ATTN: AMSTA-DDL (TECH LIBRARY) WARREN, MI 48397-5000	1
COMMANDER U.S. MILITARY ACADEMY ATTN: DEPARTMENT OF MECHANICS WEST POINT, NY 10966-1792	1
U.S. ARMY MISSILE COMMAND REDSTONE SCIENTIFIC INFO CENTER ATTN: AMSMI-RD-CS-R/DOCUMENTS BLDG. 4484 REDSTONE ARSENAL, AL 35898-5241	2
COMMANDER U.S. ARMY FOREIGN SCI & TECH CENTER ATTN: DRXST-SD 220 7TH STREET, N.E. CHARLOTTESVILLE, VA 22901	1
COMMANDER U.S. ARMY LABCOM, ISA ATTN: SLCIS-IM-TL 2800 POWER MILL ROAD ADELPHI, MD 20783-1145	1

NOTE: PLEASE NOTIFY COMMANDER, ARMAMENT RESEARCH, DEVELOPMENT, AND ENGINEERING CENTER, BENÉT LABORATORIES, CCAC, U.S. ARMY TANK-AUTOMOTIVE AND ARMAMENTS COMMAND, AMSTA-AR-CCB-O, WATERVLIET, NY 12189-4050 OF ADDRESS CHANGES.

TECHNICAL REPORT EXTERNAL DISTRIBUTION LIST (CONT'D)

	NO. OF COPIES
COMMANDER U.S. ARMY RESEARCH OFFICE ATTN: CHIEF, IPO P.O. BOX 12211 RESEARCH TRIANGLE PARK, NC 27709-2211	1
DIRECTOR U.S. NAVAL RESEARCH LABORATORY ATTN: MATERIALS SCI & TECH DIV WASHINGTON, D.C. 20375	1
WRIGHT LABORATORY ARMAMENT DIRECTORATE ATTN: WL/MNM EGLIN AFB, FL 32542-6810	1
WRIGHT LABORATORY ARMAMENT DIRECTORATE ATTN: WL/MNMF EGLIN AFB, FL 32542-6810	1

NOTE: PLEASE NOTIFY COMMANDER, ARMAMENT RESEARCH, DEVELOPMENT, AND ENGINEERING CENTER, BENÉT LABORATORIES, CCAC, U.S. ARMY TANK-AUTOMOTIVE AND ARMAMENTS COMMAND, AMSTA-AR-CCB-O, WATERVLIET, NY 12189-4050 OF ADDRESS CHANGES.